Journal of Applied Polymer Science

Preparation and Characteristic of a Sodium Alginate/Carboxymethylated Bacterial Cellulose Composite with a Crosslinking Semi-Interpenetrating Network

Qinghua Lin,[1] Yudong Zheng,[1] Lingling Ren,[2] Jian Wu,[1] Hong Wang,[1] Jiaxin An,[1] Wei Fan[1]
[1]School of Materials Science and Engineering, University of Science and Technology Beijing, Beijing 100083, People's Republic of China
[2]National Institute of Metrology of China, Beijing 100013, People's Republic of China
Correspondence to: Y. Zheng (E-mail: zhengyudong@mater.ustb.edu.cn)

ABSTRACT: A novel ionic crosslinking sodium alginate (SA)/carboxymethylated bacterial cellulose (CM-BC) composite with a semi-interpenetrating polymer network (semi-IPN) structure was developed in this study. The composite was prepared through the blending of an SA gel with CM-BC then crosslinking by Ca^{2+} followed by a freeze-drying process. Scanning electron microscopy showed the composite matrix organized in a three-dimensional network of CM-BC interpenetrated against SA molecular chains with a quantity of calcium alginate microspheres upon the surface. The swelling ratios of the composite were enhanced by 183, 198, and 212% with the supplementation of CM-BC weight fractions of 25, 50, and 75%, respectively; the swelling ratios changed with changing pH. The tensile modulus, tensile strength, and elongation at break of SA were enhanced by 165, 152, and 188%, respectively, with the addition of 50 wt % CM-BC. This study demonstrated that the semi-IPN structure dramatically changed the swelling and mechanical properties of the composite, and the semi-IPN will be a promising candidate for biomedical applications such as wound dressings and skin tissue engineering. © 2013 Wiley Periodicals, Inc. J. Appl. Polym. Sci. **2014**, *131*, 39848.

KEYWORDS: biomaterials; blends; cellulose and other wood products; composites

Received 31 May 2013; accepted 12 August 2013
DOI: 10.1002/app.39848

INTRODUCTION

In recent years, a large number of research groups have been dedicated to producing new and improved wound dressings through the synthesis and modification of biocompatible materials.[1–5] The goal of wound dressing is the production of an ideal structure, which maintains a moist environment at the wound interface, allows gaseous exchange, acts as a barrier to microorganisms, and removes excess exudates.[6] It should also be nontoxic, easily removed without trauma, and machinable. To reach this goal, wound-dressing materials must be selected carefully, and their structure must be controlled to confirm that they have has good barrier properties, swelling capacity, and mechanical properties.

Alginate is a biomaterial that has found numerous applications in biomedical science and engineering because of its favorable properties, including biocompatibility and ease of gelation. An alginate chain is composed of mannuronic acid (M units) and guluronic acid (G units), arranged in blocks rich in G units, blocks rich in M units, and blocks of alternating G and M units [Scheme 1(a)], but only G blocks can be crosslinked by ionic bonds. As alginate hydrogels gels retain a structural similarity to the extracellular matrices in tissues, they have been particularly attractive in wound healing,[7–9] drug delivery,[10–12] and tissue engineering[13,14] applications to date. However, the low mechanical performances of hydrogels and matrices limit its practical applications in the fields mentioned previously.[15,16]

Bacterial cellulose [BC; Scheme 1(b)], synthesized in abundance by *Acetobacter xylinum*, shows a high mechanical strength and remarkable physical properties that result from the unique nanostructure of the never-dried (high-water-content) membrane.[17] Because of its unique nanostructure and properties, BC is also a natural candidate for numerous medical and tissue-engineered applications.[18,19] In addition, more and more research on its derivatives has been directed toward special applications in the field of biomaterials. The synthesis of different derivatives of BC, such as by acetylation, silylation, and carboxymethylation,[20–24] with staggered degrees of substitution by various chemical treatments, could open further possibilities for new applications in different fields. For instance, carboxymethylated bacterial cellulose (CM-BC), which is soluble in water with high substitution degrees, has been used as a hemostatic

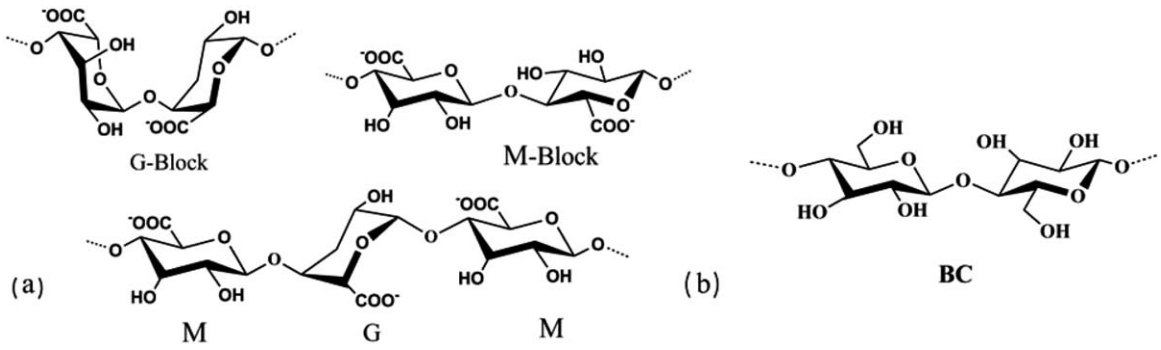

Scheme 1. Chemical structures of the (a) G-block, M-block, and alternating block in alginate and (b) cellulose molecule.

material;[25] it performs well with minor cuts but not with big wounds.

In this study, BC specimens were crushed and went through a carboxymethylation process to get CM-BC. From the mixture of the CM-BC in sodium alginate (SA) sol and crosslinking by Ca^{2+} followed by a freeze-drying process, a novel ionic crosslinking composite with semi-interpenetrating polymer network (semi-IPN) was formed to take advantage of the mild gelation performance and excellent swelling rate of SA. Meanwhile, the CM-BC gained a perfect swelling ratio and promising biomedical functions, which were proven to have an ideal mechanical reinforced phase in this semi-IPN structure. The three-dimensional microstructure, crystallinity, morphology, thermostability, swelling properties, and water-holding capacity were characterized and compared. Moreover, changes in the physical and mechanical properties caused by the addition of different CM-BC weight fractions were also tested and compared.

EXPERIMENTAL

Materials

The BC used in this study was a gel-like cellulose pellicle formed by *A. xylinum* AGR 60, which was kindly supplied by the Hainan Yida Food Co., Ltd. As a pretreatment, BC specimens were immersed in a 0.1 mol/L sodium hydroxide solution for 60 min in a 90°C water bath to remove the bacterial cell debris and were then thoroughly washed with deionized water until they were neutral. The SA used in this study was purchased from Tianjin Guangfu Fine Chemical Research Institute. The rest of the regents used in the experiments were all analytical reagents.

Preparation of the CM-BC and SA/CM-BC Composites

The CM-BCs were prepared as follows. First, the BC specimens were crushed to form a slurry with an ultrasonic cell crusher at room temperature. After three solvent exchanges of water and ethyl alcohol, the BC slurry (136 g of wet BC in 200 mL of water/ethyl alcohol) was vigorously stirred by magnetic stirrers. Then, aqueous sodium hydroxide (10%, 1200 mL) was added over 30 min at room temperature. After 2 h, 75 g of sodium chloroacetate was added over 30 min, and this mixed solution was stirred in a water bath for 5 h at 55°C. When it was cooled, we filtered the mixed solution and neutralized it with 10% acetic acid. After the repeated addition of deionized water and centrifuging, the product was obtained.

The SA and SA/CM-BC composite with a crosslinking semi-IPN were prepared. First, SA (2.0% w/v) and CM-BC were dissolved in deionized water with weight fractions of 0, 25, 50, and 75% to form a gel-like solution under thorough magnetic stirring. Then, the gel-like solutions were placed in 96-well culture plates, crosslinked by an aqueous solution of 2.0% $CaCl_2$ via a fog sprayer, and rinsed with deionized water to remove excess chlorides. Third, both of the composites were prefrozen for 12 h before they experienced a freeze-drying process for 24 h.

The degree of substitution of CM-BC was tested by acid–base titration. After vacuum drying at 110°C, 0.1 g of CM-BC was dissolved in 50 mL of water, and we added 30 mL of a 0.105 mol/L hydrochloric acid solution. Then, 1–2 drops of phenolphthalein were added after 0.5 h, and a 0.095 mol/L sodium hydroxide solution was used as a titrant until the mixed solution turned pink. The volume of the sodium hydroxide solution consumed was recorded as *V*, and the degree of substitution (DS) of CM-BC was then calculated according to the following equation:

$$\mathrm{DS} = [162m/(m - 58B)] \quad (1)$$

where B represents the molar weight of sodium hydroxide reacted with carboxyl group is equal to $(0.095V - 0.105 \times 30) \times 10^{-3}$ and m represents the weight of CM-BC.

Characterization of the CM-BC and Composites

Chemical structure information was gathered by Fourier transform infrared (FTIR) spectroscopy (Nicolet 750) with a range of frequency from 4000 to 450 cm^{-1} and a resolution of 4 cm^{-1}. The chemical structures of CM-BC and BC were tested in this way.

X-ray diffraction (XRD; D/MAX-RB, 20 kV, 40 mA) with Cu Kα radiation ($\lambda = 0.154$ nm) was used to examine the crystal structure of the samples. The range of diffraction angles (2θs) was 10–60°.

The microstructures of SA and SA/CM-BC (25, 50, and 75%) were observed by scanning electron microscopy (SEM; Apollo 300, 10 kV). All of the samples were freeze-dried and coated with a thin layer of gold in a sputter coater in advance.

Thermogravimetric analysis essays were carried out with a Shimadzu TGA 50 analyzer equipped with a platinum cell. The

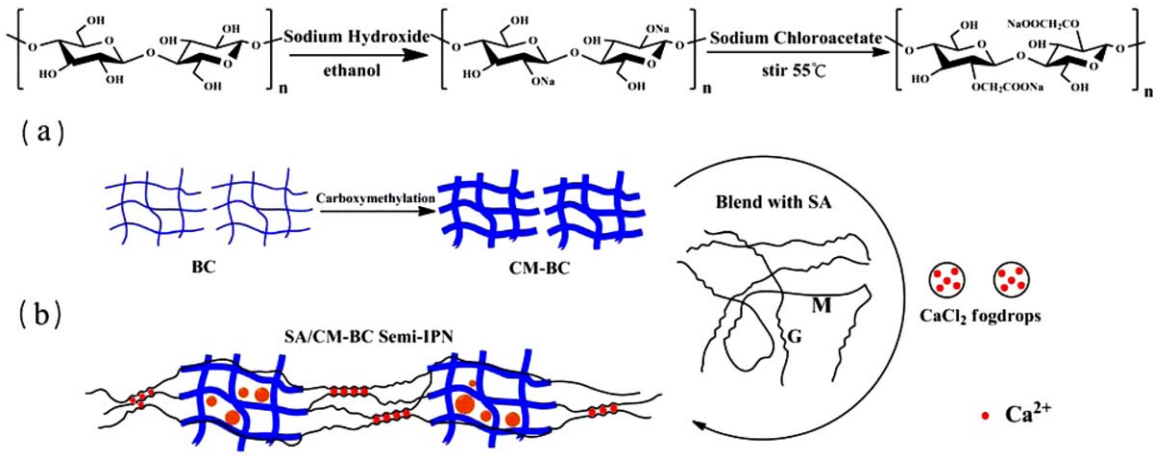

Scheme 2. Formation process for (a) the preparation of CM-BC and (b) the composite with a semi-IPN structure. [Color figure can be viewed in the online issue, which is available at wileyonlinelibrary.com.]

samples (10–15 mg) went through a freeze-drying process before they were heated at a constant rate of 10°C/min from room temperature to 800°C under a nitrogen flow of 20 mL/min. The thermal decomposition temperature was taken as the onset of significant at 5% weight loss after the initial moisture loss.

Swelling Properties and Water-Holding Capacity

To measure the swelling properties of these composites, each kind of preweighed freeze-dried sample (SA, SA/CM-BC25, SA/CM-BC50, and SA/CM-BC75, cylinder height = 5 mm, cylinder diameter = 30 mm) was immersed in deionized water for a sufficient time to completely swell up. The sheets were then taken out of the storage container with tweezers. The samples were put in a sieve, quickly shaken twice to remove the surface water, and then weighed. The SA/CM-BC50 swelling test at pH values of 2.32, 6.91, and 10.83 (adjusted by the addition of 0.1 mol/L HCl and NaOH solutions) was also carried out in this way. All testing was run in triplicate, and the equilibrium water content was determined with the following equation:

$$\text{Swelling ratio} = (W_w - W_d)/W_d \quad (2)$$

where W_w and W_d represent the weights of wet and dry samples, respectively.

When the weight of these wet sponges was measured, the composites were conditioned in a constant-temperature humidity chamber (relative humidity = 30%, 37°C) to measure the weight loss every hour; then, we evaluated the holding capacity of the composite.

Physical and Mechanical Properties

The bulk density of the composite (ρ_f) was calculated with eq. (3):

$$\rho_f = W_0/V_0 \quad (3)$$

where W_0 is the weight of the composite and V_0 is the volume of the composite, which was measured with the Buoyancy-based method of Raskin[26] and Thomson and Armstrong.[26,27] Briefly, the samples were conditioned at room temperature (25°C) for 24 h and cut into blocks approximately 2–3-cm long. They were then infiltrated with 99% ethanol in a Petri dish under near vacuum (<200 mBar) for over 5 min in a vacuum oven. Subsequently, the block sample was weighed in a 10-mL test tube and recorded as W_1 and weighed again after ethanol was filled in the tube and recorded as W_2. V_0 was calculated from eq. (4):

$$V_0 = 10 - [(W_2 - W_1)/\rho_{\text{ethanol}}] \quad (4)$$

where ρ_{ethanol} is the density of ethanol and is 0.79 g/cm^3 at room temperature. The density of the solid material that constructed the composite (ρ_s) was calculated from eq. (5):

$$\rho_s = \left\{1/\left[\mu_f/\rho_{\text{CM-BC}} - \left(1-\mu_f/\rho_{\text{SA}}\right]\right\}\right. \quad (5)$$

where μ_f is the weight fraction of CM-BC in the composite. $\rho_{\text{CM-BC}}$ and ρ_{SA} refer to the densities of CM-BC and 2 wt % SA and were 1.08 and 0.42 g/cm^3. The porosity of the composites was calculated from eq. (6):

$$\text{Porosity} = 1 - \rho_f/\rho_s \quad (6)$$

The compressive and tensile properties of the SA and SA/CM-BC composites were determined with a TA.XT Plus Texture Analyzer with the A/TG tensile grips and P/75 compression platens, respectively. Tensile and compressive experiments were performed at a speed of 2 mm/s at room temperature. The tensile samples were rectangular strips (45 × 7 × 3 mm^3), whereas the compressive samples were cylinders (15 × 13 mm^2) for the composites.

RESULTS AND DISCUSSION

Formation of the CM-BC and Composites with a Crosslinking Semi-IPN

Scheme 2(a) shows the preparation scheme for CM-BC. The DS of the product was 0.24. We mixed CM-BC in the alginate sol through strong stirring; the G blocks in different alginate chains formed ionic crosslinks through Ca^{2+} irons. Meanwhile, the CM-BC distributed in that sol was covered and fastened up between the crosslinked G blocks; this resulted in a interlaced network that consisted of calcium alginate and CM-BC. In addition, the surface of these $CaCl_2$ fog drops rained on the CM-BC were inverse-phrase crosslinked by the alginate covered

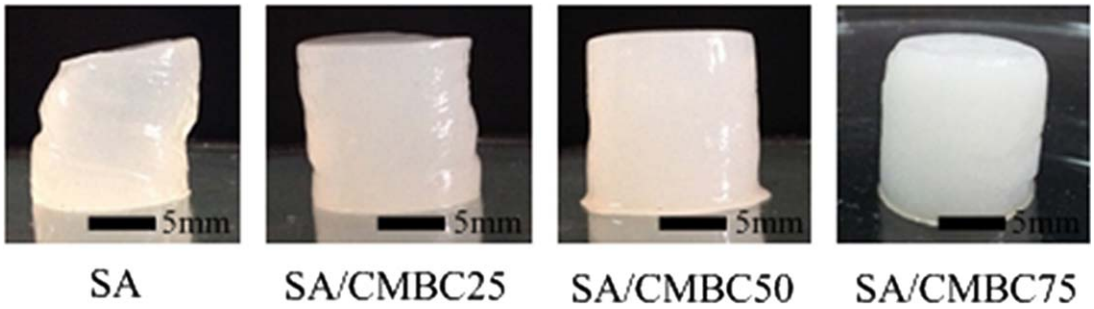

Figure 1. Photographs of SA, SA/CM-BC25, SA/CM-BC50, and SA/CM-BC75. [Color figure can be viewed in the online issue, which is available at wileyonlinelibrary.com.]

on the CM-BC and formed numbers of calcium alginate microspheres filled in the CM-BC network [Scheme 2(b)]. In this way, an SA/CM-BC composite with this special semi-IPN structure was developed.

Figure 1 shows sample pictures of SA, SA/CM-BC25, SA/CM-BC50, and SA/CM-BC75. Obviously, these hydrous cylindrical samples became more and more regular and opaque with the addition of CM-BC. Compared with the other three composites, the SA samples seemingly had the lowest bearing strength, as they could hardly stand up themselves after they were taken out of the mold, whereas the SA/CM-BC samples had good structural stability in both the hydrous and anhydrous states. Moreover, all of the samples contracted as time passed, and the percentage contraction decreased with the addition of CM-BC. Finally, all of the hydrous samples went through a freeze-drying process to remove free water inside and formed a porous structure.

Characterization of the CM-BC and Composites

SEM. The surface morphology of the BC and CM-BC are shown in Figure 2. It was obvious that the BC fiber diameters became thicker and tended to gather into bundles. Figure 2(a–d) shows the surface SEM images of the SA and SA/CM-BC25, SA/CM-BC50, and SA/CM-BC75 composites. The CM-BC was found to interpenetrate against SA molecular chains, and the surface of the SA and SA/CM-BC piled up with calcium alginate microspheres; its size fell in the range 1–5 μm. The microspheres almost covered the surface of the remaining SA without a small opening and formed a compact layer. The calcium alginate microspheres filled in the debris with the addition of CM-BC debris and CM-BC50 had many more openings on the surface than those of CM-BC25 [Figure 2(b)]. The surface microstructure of the SA/CM-BC was totally different from that of bacterial cellulose/alginate (BCA)[28,29] because of the chemical modification of BC. These microspheres may be used as drug-carrying microsphere through the blending of the drug with $CaCl_2$.

Figure 2(e–h) shows the cross-sectional SEM images of the SA and SA/CM-BC25, SA/CM-BC50, and SA/CM-BC75 composites. The SEM micrographs showed composites with a three-dimensional interconnection structure throughout; the pore size of the composites fell in the range 80–600 μm, which is suitable for use in skin tissue engineering. The cross section of SA presented a cellular-like structure [Figure 2(e)]. With increasing CM-BC, a less favorable cellular structure in the composite formed, and pore size became gradually irregular [Figure 2(g,h)].

After the ionic crosslinking and freeze-drying treatment, an SA/CM-BC composite with a crosslinking semi-IPN structure was obtained. In addition, the SA/CM-BC composites had an asymmetric structure consisting of a top skin layer and a spongelike porous layer. The existence of good biocompatibility in the CM-BC and the ill cellular structure provided great probability for applications in tissue engineering.

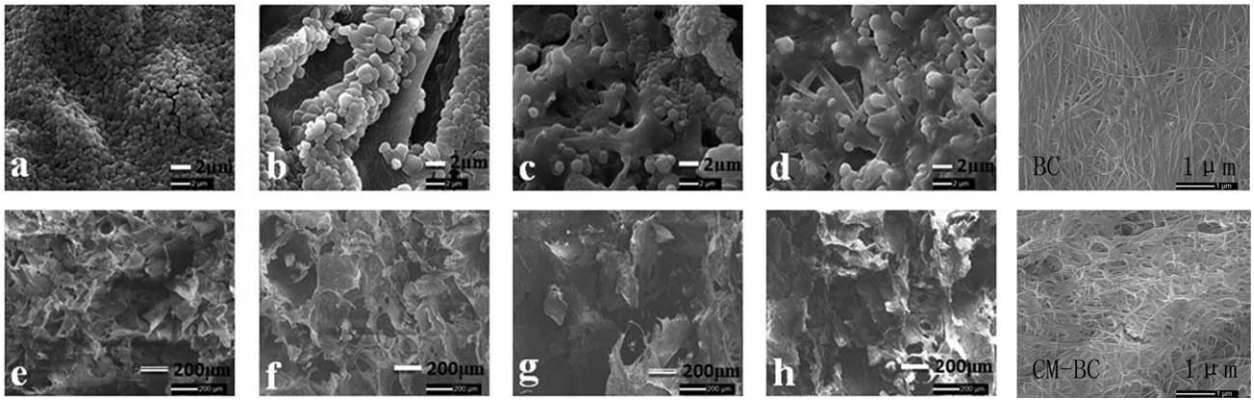

Figure 2. SEM micrographs of the BC (surface), CM-BC (surface), and SA/CM-BC composites [(top) surfaces and (bottom) cross sections] with different CM-BC weight fractions: (a,e) SA/CM-BC0, (b,f) SA/CM-BC25, (c,g) SA/CM-BC50, and (d,h) SA/CM-BC75.

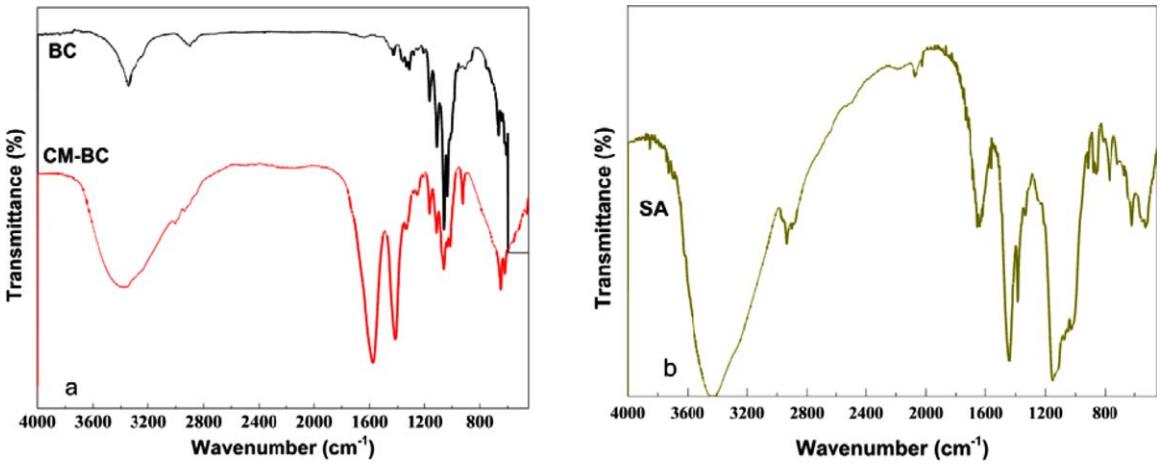

Figure 3. FTIR spectra of the (a) BC and CM-BC and (b) SA. [Color figure can be viewed in the online issue, which is available at wileyonlinelibrary.com.]

FTIR Analysis. Figure 3(a,b) shows the FTIR spectra of the CM-BC, BC, and SA. The hydroxyl groups on the BC molecular chain converted to carboxymethyl groups after carboxymethylation. For BC, there were three absorption peaks at 3370, 2900, and 1060 cm^{-1}; these peaks corresponded to the stretching vibrations of the ν(—OH), ν(—CH_2), and ν(C—O) groups, respectively. In a comparison of the FTIR curve of the original BC with that of CM-BC, new absorption peaks appeared at 1580 and 1415 cm^{-1} and were assigned to the C═O stretching vibrations of the carboxymethyl group after carboxymethylation; this indicated the successful branch joint of the carboxymethyl group on the BC molecular chain.

The SA/CM-BC composites exhibited characteristic absorption bands, with the appearance of no new peaks or the disappearance of any peaks associated with the parent molecules, as shown in Figure 4. The carboxymethyl group bands of the CM-BC were shifted from 1580 to 1540 and 1415 to 1467 cm^{-1}. This shift was attributed to intermolecular interactions between the hydroxyl groups of cellulose and carboxyl groups of SA; this might have disrupted the hydrogen bonding between CM-BC.

XRD Analysis. Figure 5 shows the XRD patterns of the BC, CM-BC, SA, and SA/CM-BC composites with CM-BC weight fractions of 25, 50, and 75. BC showed an XRD pattern with strong peaks at 2θ 14.6, 16.5, and 22.5°; this corresponded to the typical profile of a cellulose I allomorph. After carboxymethylation, the CM-BC showed characteristic 2θ peaks at 31.7 and 45.4°; this indicated that the carboxymethylation process dramatically changed the structure of BC. The XRD pattern of the SA/CM-BC composites showed typical diffraction-peak superposition of both the CM-BC nanofibers and SA, and when more CM-BC was added, the peaks at 2θ values of 31.7 and 45.4° became more pronounced.

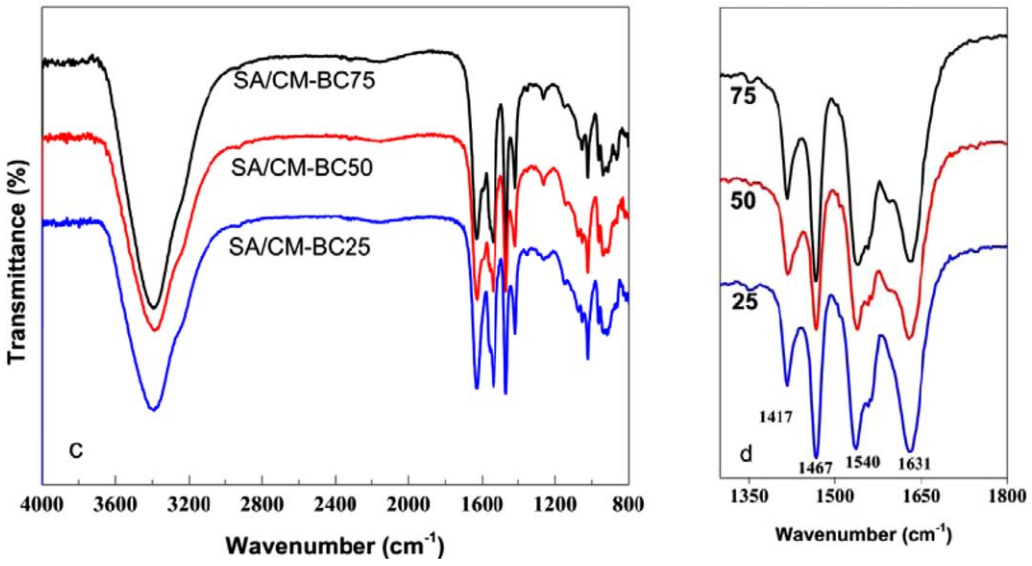

Figure 4. FTIR spectra of SA/CM-BC composites with different weight fractions ranging from (a) 800 to 3200 and (b) 1300 to 1800 cm^{-1}. [Color figure can be viewed in the online issue, which is available at wileyonlinelibrary.com.]

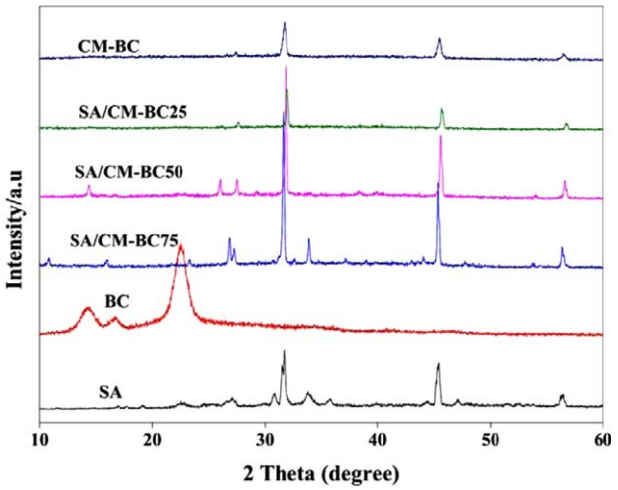

Figure 5. XRD patterns of the BC, CM-BC, SA/CM-BC composites with different CM-BC weight fractions, and SA. [Color figure can be viewed in the online issue, which is available at wileyonlinelibrary.com.]

Thermal Properties. Thermogravimetric analysis of the composites was carried out to assess their thermal stability and degradation profiles. Similar to that of BC, the thermogravimetry (TG) curve of CM-BC exhibited three distinct decomposition steps. The first corresponded to water loss, whereas the second was attributed to the decomposition of the cellulose backbone. The TG curves of both SA/CM-BC composites revealed that there were two weight loss steps that were related to the water elimination and the thermal degradation of both CM-BC and SA [Figure 6(a,b)].

The onset degradation temperatures of SA, BC, CM-BC, SA/CM-BC25, SA/CM-BC50, and SA/CM-BC75 were 146, 252, 243, 165, 178, and 187°C, respectively. It was obvious that the onset degradation temperature of BC declined after carboxymethylation, and the residues increased at the same time; this could have been due to the breaking of the fiber of BC and the emergence of carboxymethyl groups on the BC molecular chain. The composites showed lower onset degradation temperatures than the CM-BC because of the loss of intermolecular hydrogen bonds of cellulose by the presence of SA. On the other hand, the SA deposited on the CM-BC fiber surface started to decompose at higher temperatures (increasing to 15, 32, and 41°C) when compared with pure SA. Moreover, the increase in the CM-BC content resulted in considerable increases in the maximum degradation temperature of 49, 57, and 99°C, respectively [Figure 6(b)]. Both phenomena could be explained by the higher stability of the CM-BC fiber substrates and, particularly, by the excellent compatibility between the two carbohydrate components of the composites. In addition, in the TG curves, except for CM-BC, all of the other samples presented a residual mass of about 60% or more; this may have been due to the SA gel coating on the fiber chain, which delayed the degradation process. Compared with other cellulose substrates in the polymeric matrices,[30,31] regardless of the fact that higher reinforcing agent contents were normally used, the effects observed were much less pronounced than the values reported here.

Swelling Properties and Water-Holding Capacity

Figure 7(a) shows the swelling ratio of SA/CM-BC with different CM-BC weight fractions. The SA swelled rapidly and achieved a quick equilibrium within 3–4 min. The finally weight was approximately 6.6 times its weight in dry. The supplement of CM-BC, which had an excellent water absorption capacity (14.7 times its dry weight), resulted in an increase in the swelling ratio but slowed down the process of swelling. For example, the equilibrium weights of SA/CM-BC25, SA/CM-BC50, and SA/CM-BC75 were 12.1, 13.0, and 14.0%, respectively, of their dry weight but took about 5, 7, and 12 min, respectively, to achieve equilibrium, as shown in Figure 7(b). It has been reported that blending with alginate could disrupt the hydrogen bonding between the CM-BC; this may have been another for the increase in the swelling ability. The investigation of the SA/CM-BC50 composite swelling behavior as a function of time was also performed in phosphate buffer at pH 2.32, 6.91, and 10.83 [Figure 7(c)]. It was obvious from their dynamic swelling profiles that the alkaline condition led to swelling, whereas the acidic condition lowered the swelling degree. That was precisely attributed to the reduced osmotic pressure of the network for swelling due to protonation of carboxyl groups, which resulted in a decrease in the free counterions of Na^+.

Figure 7(d) shows the water-holding capacities of SA/CM-BC with different CM-BC weight fractions. The water-holding

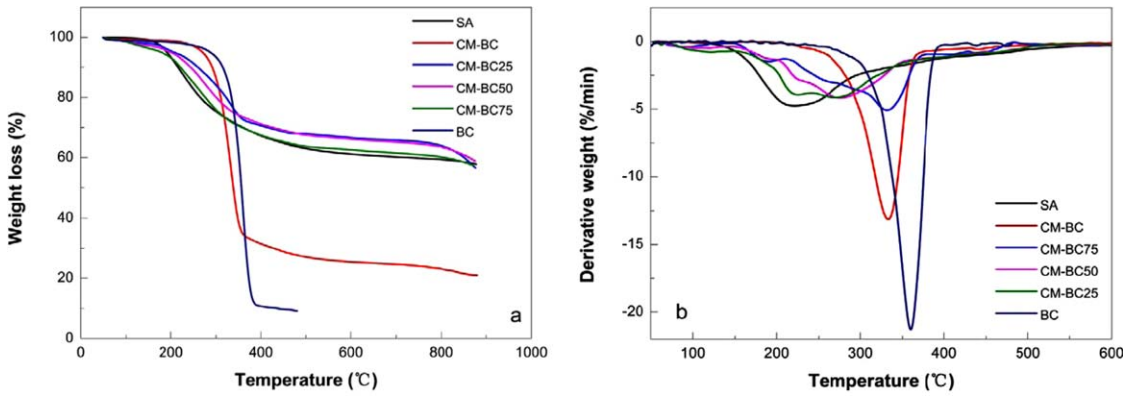

Figure 6. (a) TG and (b) derivative TG curves for the SA, BC, CM-BC, and SA/CM-BC composites. [Color figure can be viewed in the online issue, which is available at wileyonlinelibrary.com.]

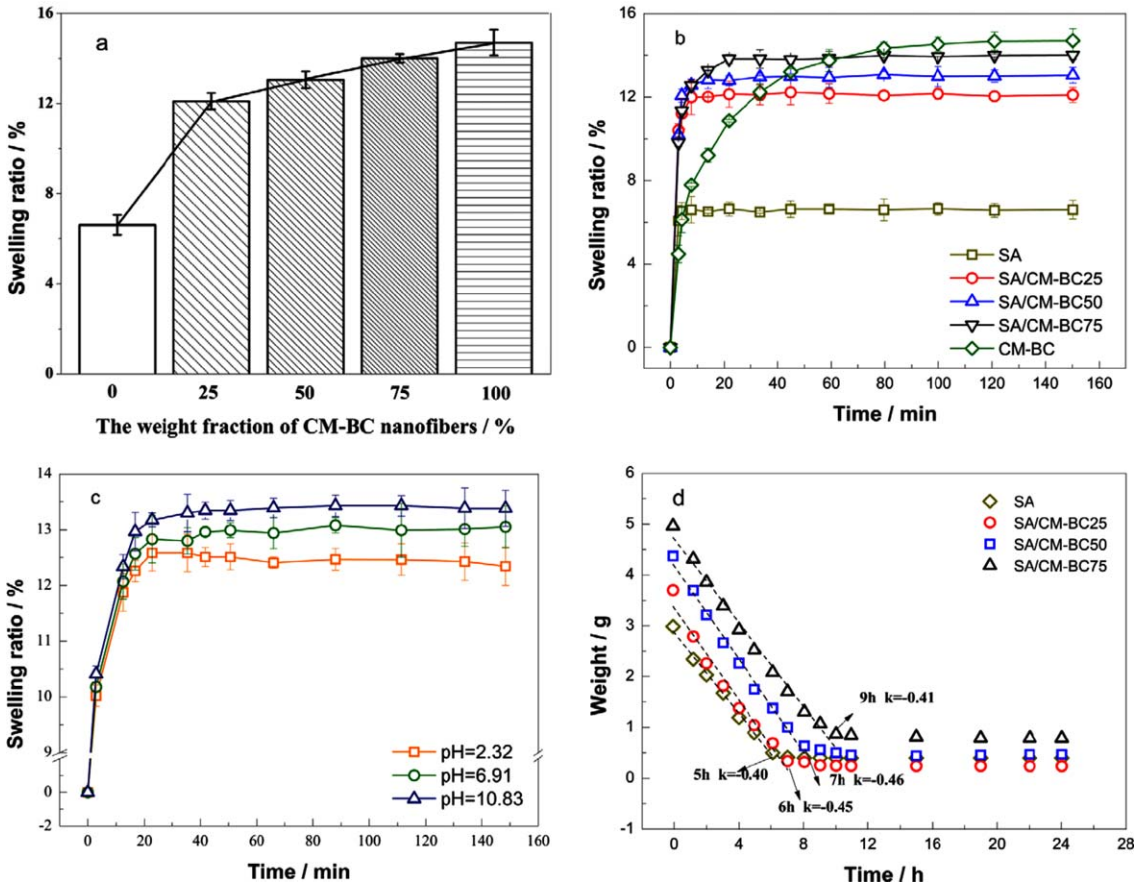

Figure 7. Swelling behaviors of the SA/CM-BC composites: (a) maximum swelling ratio, (b) swelling behaviors at pH 7.0 with different CM-BC weight fractions, (c) swelling behaviors of SA/CM-BC50 at different pHs, and (d) water loss behaviors of the SA/CM-BC composites with different CM-BC weight fractions, where k represents the gradient of the fitted lines. [Color figure can be viewed in the online issue, which is available at wileyonlinelibrary.com.]

capacity of composites is also an important criterion in many practical applications. The results of the water-holding capacity experiments, performed at 30% relative humidity and 37°C, showed an increase in the water-holding time and almost the same rates of water loss with the supplementation of CM-BC in the composites. The SA/CM-BC25, SA/CM-BC50, and SA/CM-BC75 composites achieved adsorption equilibrium after 8, 9, and 10 h, respectively, whereas the performance of SA approached equilibrium after about 6.5 h. Obviously, the water-holding capacity increased with the supplementation of CM-BC.

Physical and Mechanical Properties

The SA and SA/CM-BC (25, 50, and 75) composites were subject to both compressive and tensile tests. Typical stress–strain curves of the samples are depicted in Figure 8(a,b). The changes in the compressive and tensile properties of the composites

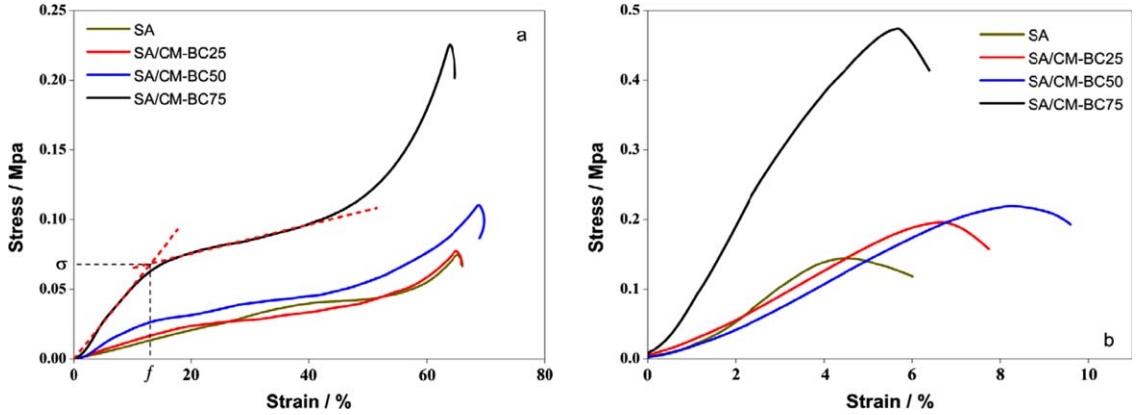

Figure 8. Mechanical properties of the SA and SA/CM-BC: (a) compressive stress–strain graphs and (b) tensile stress–strain graphs, where σ is compressive strength, the corresponding strain is f. [Color figure can be viewed in the online issue, which is available at wileyonlinelibrary.com.]

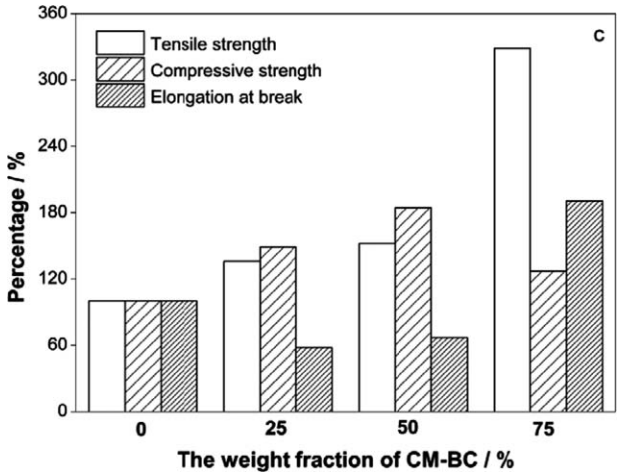

Figure 9. Changes in the properties of SA induced by the addition of CM-BC.

induced by the addition of CM-BC are summarized in Figure 9. The data of the physical and mechanical properties of both materials are summarized in Table I.

As shown in Figure 8(a), the compressive stress–strain curves showed linear elasticity at low strains, followed by a plateaulike region, and approached a cellular solid structure.[32] The compressive strength was determined from the intersection point of the linear line for obtaining the compressive modulus and the linear regression of the collapse plateau regime. When the cells had almost completely collapsed, the opposing cell walls were in contact, and further strain compressed the solid itself. This was the densification regime in which the stress rose steeply with strain. The stress–strain curve of SA moved upward with the addition of CM-BC in both tests; this indicated the enhancement of the compression modulus but a decrease in the compressive strength due to a less favorable cellular structure. However, the toughness was obviously enhanced as the maximum compressive increased hugely and changed the brittleness of SA.

Figure 8(b) shows the tensile stress–strain graphs of the SA and SA/CM-BC composites. For SA/CM-BC25, SA/CM-BC50, and SA/CM-BC75, the tensile strengths were 136, 152, and 329% of the original values for SA (Table I). Both of the materials showed elastic deformation only under strains of about 0.025% in the tensile tests. The reduction in the tensile modulus from CM-BC50 to CM-BC75 might have been due to the better CM-BC dispersion in the former, which was favorable for load transfer. The elongation at break showed the same behavior; it increased in ductility with the presence of CM-BC but not CM-BC75 (Table I). Obviously, SA played the adhesive role and held CM-BC together; the decrement of SA led to a decrease in the cohesive force and, thus, the ductility of this composite. Notwithstanding, even in CM-BC75, the elongation at break was still higher than that of SA. With the supplementation of CM-BC, the porosity increased and led to a much smaller (Table I) and irregular, ill-defined cellular structure in the composite. Similar to this phenomenon, the porosity of the BC/chitosan composite[33] demonstrated the same regularity as well but was higher (ca. 97%). In addition, it was surprising that the change rules of the compressive and tensile strength were opposite for the CM-BC/SA composite (similar to BCA[34]), both of these two mechanical properties declined with the supplementation of CM-BC, but when the content of CM-BC was up to 75%, they increased significantly.

However, the mechanical properties of this composite did not decrease but rather improved dramatically. This may indicate that these irregular ill-defined cellular had a much better bearing capacity with the existence of CM-BC.

CONCLUSIONS

From the blending of SA with CM-BC and then crosslinking by calcium ions followed by a freeze-drying process, one novel composite was prepared, in which the CM-BC interpenetrated against SA molecular chains and formed a semi-IPN. The swelling ratios of SA were enhanced by 183, 198, and 212%, respectively, with the addition of CM-BC25, CM-BC50, and CM-BC75 without any obvious changes in the water-holding capacity. The tensile modulus, tensile strength, and elongation at break were improved by 165, 152, and 188% with the addition of CM-BC50. The increase in these properties was attributed to the formation of the crosslinking semi-IPN, which showed a compact ionic crosslinking surface and a tough, ill-defined cellular structure with the addition of CM-BC. The formation of this special structure dramatically improved the swelling and thermal and mechanical properties of the composite. Further work on its biodegradation, cellular biocompatibility, and blood compatibility is underway to determine this material's practical applicability in wound dressings and skin tissue engineering.

ACKNOWLEDGMENTS

This study was financially supported by the National Natural Science Foundation of China Project (contract grant numbers 51073024 and 51273021) and the National Science and Technology

Table I. Physical and Mechanical Properties of the SA/CM-BC Composites

Sample	ρ_s (g/cm^3)	ρ_s/ρ_f	Porosity (%)	Elongation at break (%)	Tensile *E* (MPa)	Compressive *E* (MPa)	Tensile strength (kPa)	Compressive strength (kPa)
SA	0.42	0.22	78.3	4.47	1.41 ± 0.08	0.10 ± 0.01	144.25 ± 1.17	37.10 ± 1.01
SA/CM-BC25	0.50	0.15	84.6	6.66	2.29 ± 0.03	0.14 ± 0.03	195.91 ± 1.24	21.49 ± 2.43
SA/CM-BC50	0.61	0.14	85.1	8.24	2.33 ± 0.03	0.25 ± 0.05	219.66 ± 1.13	24.86 ± 4.54
SA/CM-BC75	0.78	0.10	89.8	5.68	2.15 ± 0.01	0.56 ± 0.01	474.33 ± 2.09	70.72 ± 2.66

E represents the modulus.

Support Project of China (contract grant number 2011BAK15B04).

REFERENCES

1. Rinaudo, M. *Prog. Polym. Sci.* **2006**, *31*, 603.
2. Ramli, N. A.; Wong, T. W. *Int. J. Pharm.* **2011**, *403*, 73.
3. Mi, G.-W.; Shyu, S.-S. *Biomaterials* **2001**, *22*, 165.
4. Kumar, M. N. V. R. *React. Funct. Polym.* **2000**, *46*, 1.
5. Chiaoprakobkij, N.; Sanchavanakit, N.; Subbalekha, K. *Carbohydr. Polym.* **2011**, *85*, 548.
6. Jayakumar, R.; Prabaharan, M. *Biotechnol. Adv.* **2011**, *29*, 322.
7. Gilchrist, T.; Martin, A. M. *Biomaterials* **1983**, *4*, 317.
8. Fraser, R.; Gilchrist, T. *Biomaterials* **1983**, *4*, 222.
9. Suzuki, Y.; Tanihara, M. *J. Biomed. Mater. Res.* **1999**, *48*, 522.
10. Ishak, R. A. H.; Awad, G. A. S.; Mortada, N. D.; Nour, S. A. K. *J. Controlled Release* **2007**, *119*, 207.
11. Chang, C. H.; Lin, Y. H.; Yeh, C. L.; Chen, Y. C.; Chiou, S. F.; Hsu, Y. M.; Chen, Y. S.; Wang, C. C. *Biomacromolecules* **2010**, *11*, 133.
12. Rinaudo, M. *Prog. Polym. Sci.* **2006**, *31*, 603.
13. Lee, J.; Bhang, S. H.; Park, H.; Kim, B. S.; Lee, K. Y. *Pharm. Res.* **2010**, *27*, 767.
14. Kolambkar, Y. M.; Dupont, K. M.; Boerckel, J. D. *Biomaterials* **2011**, *32*, 65.
15. Drury, J. L.; Dennis, R. G.; Mooney, D. *J. Biomaterials* **2004**, *25*, 3187.
16. Tanaka, Y.; Gong, J. P.; Osada, Y. *Prog. Polym. Sci.* **2005**, *30*, 1.
17. Backdahl, H.; Helenius, G.; Bodin, A. *Biomaterials* **2006**, *27*, 2141.
18. Czaja, W.; Krystynowicz, A.; Bielecki, S.; Brown, R. M., Jr. *Biomaterials* **2006**, *27*, 145.
19. Backdahl, H.; Helenius, G.; Bodin, A.; Nannmark, U. *Biomaterials* **2006**, *27*, 2141.
20. Geyer, U.; Heinze, T.; Stein, A.; Klemm, D. *Int. J. Biol. Macromol.* **1994**, *16*, 343.
21. Klemm, D.; Schumann, D.; Udhardt, U. *Prog. Polym. Sci.* **2001**, *26*, 1561.
22. Chen, S.; Zou, Y.; Yan, Z. *J. Hazard. Mater.* **2009**, *161*, 1355.
23. Hui, W.; Chen, S.; Xui, Q.; Wang, H. *Carbohydr. Polym.* **2011**, *83*, 1575.
24. Schlufter, K.; Schmauder, H.-P.; Dorn, S. *Macromol. Rapid Commun.* **2006**, *27*, 1670.
25. Qi, H. W. *China Foreign Med. Treat.* **2011**, *35*, 30.
26. Raskin, I. *Funct. Ecol.* **1983**, *18*, 683.
27. Thomson, C. J.; Armstrong, W. *Plant Cell Environ.* **1990**, *13*, 395.
28. Phisalaphong, M.; Suwanmajo, T. *J. Appl. Polym. Sci.* **2008**, *107*, 3419.
29. Kanjanamosit, N.; Muangnapoh, C.; Phisalaphong, M. *J. Appl. Polym. Sci.* **2010**, *115*, 1581.
30. Martins, I. M. G.; Magina, S. P.; Oliveira, L. *Compos. Sci. Technol.* **2009**, *69*, 2163.
31. Trovatti, E.; Oliveira, L.; Freire, C. S. R. *Compos. Sci. Technol.* **2010**, *70*, 1148.
32. Gibson, L. J.; Ashby, M. F. Cellular Solids: Structure and Properties; Cambridge University Press: Cambridge, United Kingdom, **1997**.
33. Liu, S.; Jeannes, S.; Chen, B. *J. Biomater. Tissue Eng.* **2011**, *1*, 60.
34. Kirdponpattara, S.; Phisalaphong, M. *Biochem. Eng. J.* **2013**, *77*, 103.